Cancer pain and neuropathic pain are associated with Aβ sensory neuronal plasticity in dorsal root ganglia and abnormal sprouting in lumbar spinal cord

Yong Fang Zhu[1,2], Jacek M Kwiecien[2,3], Wojciech Dabrowski[4], Robert Ungard[1,2], Kan Lun Zhu[2], Jan D Huizinga[5], James L Henry[6], and Gurmit Singh[1,2]

Abstract

Evidence suggests that there are both nociceptive and neuropathic components of cancer-induced pain. We have observed that changes in intrinsic membrane properties and excitability of normally non-nociceptive Aβ sensory neurons are consistent in rat models of peripheral neuropathic pain and cancer-induced pain. This has prompted a comparative investigation of the intracellular electrophysiological characteristics of sensory neurons and of the ultrastructural morphology of the dorsal horn in rat models of neuropathic pain and cancer-induced pain. Neuropathic pain model rats were induced with a polyethylene cuff implanted around a sciatic nerve. Cancer-induced pain model rats were induced with mammary rat metastasis tumour-1 rat breast cancer or MATLyLu rat prostate cancer cells implanted into the distal epiphysis of a femur. Behavioural evidence of nociception was detected using von Frey tactile assessment. Aβ-fibre low threshold mechanoreceptor neurons in both cancer-induced pain and neuropathic pain models exhibited slower dynamics of action potential genesis, including a wider action potential duration and lower action potential amplitude compared to those in control animals. Enhanced excitability of Aβ-fibre low threshold mechanoreceptor neurons was also observed in cancer-induced pain and neuropathic pain models. Furthermore, both cancer-induced pain and neuropathic pain models showed abundant abnormal axonal sprouting in bundles of myelinated axons in the ipsilateral spinal laminae IV and V. The patterns of changes show consistency between rat models of cancer-induced pain and neuropathic pain. These findings add to the body of evidence that animal models of cancer-induced pain and neuropathic pain share features that may contribute to the peripheral and central sensitization and tactile hypersensitivity in both pain states.

[1]Michael G. DeGroote Institute for Pain Research and Care, McMaster University, Hamilton, ON, Canada
[2]Department of Pathology and Molecular Medicine, McMaster University, Hamilton, ON, Canada
[3]Department of Clinical Pathomorphology, Medical University of Lublin, Lublin, Poland
[4]Department of Anaesthesiology and Intensive Therapy, Medical University of Lublin, Lublin, Poland

[5]Department of Medicine, Farncombe Family Digestive Health Research Institute, McMaster University, Hamilton, ON, Canada
[6]Department of Psychiatry and Behavioural Neurosciences, McMaster University, Hamilton, ON, Canada

Corresponding Author:
Gurmit Singh, McMaster University, 1280 Main Street West, MDCL 2102, Hamilton, ON L8S4K1, Canada.
Email: singhg@mcmaster.ca

Introduction

Pain is one of the most common symptoms reported by late-stage patients with metastatic cancer, particularly in patients with metastatic cancers in the bone.[1,2] Understanding the neurobiological mechanisms underlying cancer pain is a prerequisite for improving mechanism-based management. Murine models have contributed greatly to unravelling the central and peripheral pathological processes that contribute to inducing and maintaining neuropathic and cancer pain. This includes algogenic substances released by tumours and associated immune cells, the dysregulated activity of bone cells in proximity to the tumour, and multiple neuropathological processes including pathological sensory neuronal growth and signalling.[3,4] This diverse and complex pathological environment contributes to the features that have led to the classification of cancer pain as a unique pain state with both nociceptive and neuropathic features.[5,6]

Previous studies with murine models of cancer pain have shown changes in the functional properties of sensory dorsal root ganglion (DRG) neurons and neurons of the dorsal horn of the spinal cord[7–11]; however, the specific association of these changes with different sensory aspects of cancer pain has yet to be classified. In this study, we have described changes in the function and structure of peripheral sensory neurons in rat models of cancer pain and neuropathic pain (NEP). These changes are discussed relative to each other and their respective controls.

In our recent studies on a syngeneic rat model of prostate cancer-induced pain (CIP) in male Copenhagen (CP) rats, we observed that changes in intrinsic membrane properties and excitability of normally non-nociceptive myelinated Aβ sensory neurons follow a variable trajectory over two weeks following model induction.[11] The patterns of these changes exhibited consistency with patterns in models of NEP induced by sciatic nerve cuff in male Sprague-Dawley (SD) rats,[12] suggesting the potential for common physiological mechanisms for NEP induced by sciatic nerve cuff and CIP induced by intrafemoral implantation of cancer cells. In this study, we conducted in vivo intracellular electrophysiological experiments in DRG neurons of two rat models of CIP (male rats implanted with a prostate cancer cell line, and female rats implanted with a breast cancer cell line) and a female rat model of NEP to compare similarities and differences in the functional properties of the axons and somata of primary sensory neurons relative to their respective controls. In addition, in contrast to earlier investigations that utilize neuronal tracing, we utilized transmission electron microscopy to observe pathophysiological changes in the dorsal horn of the spinal cord at the L4 level consistent with axonal

sprouting. No analyses in this manuscript were performed to compare male CP with female SD models, as sex and strain differences limit their comparative validity. The relevant comparisons to our conclusions were not between strains, but rather in observing that those individual groups differed from their relative controls in similar measures. This study describes our observations of similar changes in two different models of distinct pain states: CIP and NEP.

We report here that the patterns of Aβ sensory neuron plasticity in the DRG and abnormal axonal sprouting in the dorsal horn of the lumbar spinal cord were similar between rat models of CIP and NEP. These peripheral and central nervous system (CNS) changes are suggested to arise alongside the progression of these chronic painful conditions and may be associated with an induction of hypersensitivity observed in both animal models of pain.

Methods

All experimental procedures conformed to the Guide to the Care and Use of Laboratory Animals, Volumes 1 and 2, of the Canadian Council on Animal Care, and all protocols were reviewed and approved by the McMaster University Animal Research Ethics Board.

Cell culture

Mammary rat metastasis tumour (MRMT-1) rat mammary carcinoma cells were kindly provided by Dr Philippe Sarret of the Université de Sherbrooke, Sherbrooke, QC. MatLyLu (MLL) rat prostate adenocarcinoma cells were obtained from the American Type Culture Collection, Manassas, VA. Cells were maintained in a humidified incubator at 37°C with 5% CO_2 in room air in growth medium supplemented with 10% fetal bovine serum and 1% antibiotic/antimycotic) (Life Technologies, Carlsbad, CA). MRMT-1 cells were grown in Roswell Park Memorial Institute 1640 medium (Life Technologies) and MLL in Dulbecco's Modified Eagle's medium growth media (Life Technologies) and tested for mycoplasma contamination prior to experimental use.

Cancer pain model induction

Male CP rats (Harlan Laboratories Inc., Indianapolis, IN) weighing 200–250 g were utilized for all prostate cancer models, and female SD rats (Charles River Inc. St. Constant, QC) weighing 170–200 g were utilized for all breast cancer models. Rats were randomly assigned to CIP or sham surgery groups. All group sizes were (n = 8) each. Rats were anaesthetised with inhaled isoflurane (3–5% in oxygen), and 3.0×10^4 MRMT-1 murine breast cancer cells for SD rats or 5.0×10^6

MATLyLu (MLL) murine prostate cancer cells for CP rats suspended in 50 μL phosphate-buffered saline were percutaneously injected into the distal epiphysis of the right femur, as described previously.[13] Sham-surgery control rats received an injection by the same procedure of heat/freeze killed cells at the same concentration and volume as the respective CIP model animals. The volume of injected material was minimized to ensure that it remained within the intramedullary space of the femur, and surgical procedures were minimized to reduce the confounding influence of pain resulting from bone and soft tissue damage.

NEP model induction

Female SD rats weighing 170–200 g were used for NEP models (n = 8). A peripheral neuropathy was induced by the "sciatic cuff model" according to methods previously described in detail.[12,14–18] Animals were anaesthetised with a mixture of ketamine (Narketan; 5 mg/100 g; Vetoquinol N.-A. Inc.; Lavaltrie, QC), xylazine (Rompun; 0.5 mg/100 g; Bayer Inc., Toronto, ON) and acepromazine (Atravet; 0.1 mg/100 g; Ayerst Veterinary Laboratories, Guelph, ON) given intraperitoneally, and the right sciatic nerve was exposed at the mid-thigh level. Two cuffs of 0.5 mm polyethylene (PE 90) tubing (Intramedic PE-90, Fisher Scientific Ltd., Whitby, ON) were inserted around the exposed nerve 1 mm apart. The muscle and skin of the wound were then sutured separately. Antibiotic ointment (Furacin, nitrofurazone 0.2%; Vetoquinol N.-A. Inc.) was applied over the wound, and 0.01 ml/100 g of antibacterial injectable solution (Baytril; Bayer Inc.) was injected subcutaneously.

Von Frey test of paw withdrawal threshold

Behavioural tests were performed on post-surgical days 21–27, immediately prior to anaesthesia for electrophysiological recordings to quantify the development of the tactile hypersensitivity that is characteristic of NEP and CIP. Rats were placed in a transparent Plexiglas box with 0.5 cm diameter holes spaced 1.5 cm apart on the floor to allow full access to the paw.[12,15,19] Animals were allowed to habituate to the box until cage exploration and major grooming activities had ceased.

Von Frey filaments (Stoelting Co., Wood Dale, IL) were applied to the plantar surface of the ipsilateral hind paw to determine mechanical withdrawal thresholds using the up-down method of Dixon.[20] A von Frey filament was applied 5 times for 3–4 s each at 3-s intervals to a different spot on the plantar surface of the ipsilateral hind paw. Filaments were applied in ascending order of force until a clear withdrawal response was observed. When this occurred, the next lightest filament was re-applied, and the process continued until a 50% withdrawal response threshold was derived.[21] Brisk foot withdrawal in response to the mechanical stimulus was interpreted as indicating a valid response.

Intracellular DRG recording in vivo

Details of acute intracellular electrophysiological recording techniques have been reported previously in animal models of NEP.[12,18,19] Briefly, each rat was initially anaesthetised with a mixture of ketamine, xylazine and acepromazine delivered intraperitoneally on post-surgical days 21–27. The right jugular vein was cannulated for intravenous infusion of drugs, and the rat was fixed in a stereotaxic frame with the vertebral column rigidly clamped at L2 and L6. The L4 DRG was selected for study, as it contains large numbers of hind leg afferent somata. A laminectomy was performed to expose the ipsilateral L4 DRG. The L4 dorsal root was sectioned close to the spinal cord and placed on a bipolar electrode (FHC, Bowdoinham, ME) used for stimulation. The exposed spinal cord and DRG were covered with paraffin oil at 37°C to prevent drying. Rectal temperature was measured and maintained at 37°C using a temperature-controlled infrared heating lamp.

For recording, each rat was maintained at a surgical level of anaesthesia using sodium pentobarbital (20 mg/kg; Ceva Sante Animal, Libourne, France) and was mechanically ventilated via a tracheal cannula using a Harvard Ventilator (Model 683, Harvard Apparatus, QC). The ventilation parameters were adjusted so that end-tidal CO_2 concentration was maintained at 40–50 mmHg, as measured using a CapStar-100 End-Tidal CO_2 analyser (CWE, Ardmore, PA). Immediately before the start of recording, an initial 1 mg/kg dose of pancuronium (Sandoz, Boucherville, QC) was given to eliminate muscle tone. The effects of pancuronium were allowed to wear off periodically to confirm a surgical level of anaesthesia; this was monitored by observing pupil diameter and response to a noxious pinch of a forepaw. Supplementation of sodium pentobarbital and pancuronium was administered at doses of 1/3 of the previous dose, approximately each hour via the jugular cannula.

Intracellular recordings from somata in the exposed DRG were made with borosilicate glass micropipettes (1.2 mm outside diameter, 0.68 mm inside diameter; Harvard Apparatus, Holliston, MA). The electrodes were pulled using a Brown-Flaming pipette puller (model P-87; Sutter Instrument Co., Novota, CA). These electrodes were filled with 3 M KCl (DC resistance 50–70 MΩ). Signals were recorded with a Multiclamp 700B amplifier (Molecular Devices, Union City, CA) and digitized online via Digidata 1322A interface (Molecular Devices) with pClamp 9.2 software

(Molecular Devices). The microelectrode was advanced using an EXFO IW-800 micromanipulator (EXFO, Montreal, QC) in $2\,\mu m$ steps until an abrupt hyperpolarization of at least $40\,mV$ appeared. Once a stable membrane potential had been confirmed, a single stimulus was applied to the dorsal root to provoke an action potential (AP). The protocol editor function in the pClamp 9.2 software was used to evoke a somatic AP by stimulation with a single rectangular intracellular depolarizing voltage pulse.

AP configuration and conduction velocity

The first AP evoked by stimulation of the dorsal root and measured at the DRG soma in each neuron was used to compare the configuration parameters between control and model rats. Criteria for inclusion of neurons in the subsequent analysis included a stable resting membrane potential (Vm) more negative than $-40\,mV$ with a somatic spike evoked by dorsal root stimulation that was $>40\,mV$. Variables in AP configuration included Vm, action potential amplitude (APA), AP duration at base (APdB), action potential rise time (APRT), action potential fall time (APFT), afterhyperpolarization amplitude (AHPA), and afterhyperpolarization duration to 50% recovery (AHP50). The distance from the stimulation site (cathode) to the recording site (centre of the DRG) was measured at the end of the experiment to determine the conduction distance. This value was used to calculate the conduction velocity (CV) of the dorsal root axon associated with each neuron.

DRG neuron classification

Recorded neurons were classified as $A\beta$-fibre neurons based on their AP configuration, CV, and their receptive field properties defined by using hand-held mechanical stimulators.[12,22,23] The differentiation of high threshold mechanoreceptor (HTM) neurons versus low threshold mechanoreceptor (LTM) neurons was based on their sensory properties identified during receptive field searching. HTM neurons responded to noxious stimuli including noxious pressure, pinch and probing with fine forceps, sharp needle, coarse-toothed forceps, or coarse flat forceps, whereas LTM neurons responded to innocuous stimuli such as a moving brush, light pressure with a blunt object, light manual tap or vibration. In addition to the threshold of activation, the rate of adaption and the tissue location of the receptive field, other major factors were used to further classify $A\beta$-fibre LTM neurons as cutaneous neurons (CUT) or muscle spindle (MS) neurons. The CUT neurons included guard/field hair neurons (GF), glabrous skin neurons, Pacinian neurons and slowly adapting (SA) neurons. GF neurons were rapidly adapting (RA) CUT. Glabrous and Pacinian neurons were both RA non-hair neurons and were named RA neurons. SA neurons were SA CUT. MS neurons were SA neurons with deep subcutaneous receptive fields activated by deep tissue manipulation of the muscle belly but not by cutaneous stimulation. Only data from $A\beta$-fibre LTM neurons were included in this study.

Excitability of DRG neurons

Excitability was measured by evoking APs in the somata of the DRG neurons using three stimulation techniques: stimulation of the soma by direct injection of depolarizing current, electrical stimulation of the dorsal roots using bipolar stimulating electrodes, and mechanical stimulation of the peripheral receptive field.[18] To quantify soma excitability, the threshold of depolarizing current pulses injected into the soma was determined by applying pulses of $100\,ms$ in increments of $0.05\,nA$ through the recording electrode until an AP was elicited or until a maximum current of $4\,nA$ was reached. The excitability of the soma was also evaluated by comparing the number of APs evoked by injecting defined current pulses to the DRG soma; three intracellular current injections of $100\,ms$ each were delivered with 1 and $2\,nA$ amplitude. Dorsal root excitability was measured by determining the chronaxie curve (threshold-duration), which was determined by delivering the minimum current that would elicit an AP in the soma to the dorsal root using current pulse durations of 0.2, 1, 2, 4 and $6\,ms$. The stimulation pulse was delivered from an S940/910 stimulus adaptor/isolator (Dagan, Minneapolis, MN).

Ultrastructural analysis of the lumbar spinal cord

For ultrastructural analyses, samples were analysed from CP CIP-model rats (n = 4), CP sham control rat (n = 1), SD NEP rats (n = 3) and SD sham control rat (n = 1). For whole-body perfusion, rats were deeply anaesthetized with an intraperitoneal injection of $100\,mg/kg$ sodium pentobarbital (Ceva Sante) and the chest opened. A dose of 100 IU heparin sodium was injected into the left ventricle, and a cannula inserted into the left ventricle, while the right auricle was cut to allow for wash-out of blood with lactated Ringer's solution followed by Karnowski's fixative for histology and electron microscopy.[24] The tissues of the spinal cord were carefully removed and post-fixed in Karnowski's fixative. A cross-section of the lumbar spinal cord at L4 was collected and used for morphological analyses. For light microscopy, 1-μm-thick epon-embedded sections were cut with a glass knife, mounted on a glass slide and stained with toluidine blue. These sections were analysed under a Nikon Eclipse 50i microscope.

Silver grey ultrathin sections from epon-embedded portions of the spinal cord were cut at 40 nm thick and mounted on Formvar-coated copper grids, stained with uranyl acetate and lead citrate and examined under a Jeol 1200EX Biosystem transmission electron microscope. Multiple digital photographs of the white matter tracts within the right dorsal horn were taken at 5000–40,000× magnification from several non-overlapping areas of the dorsal root that contained clusters of small unmyelinated axonal profiles. Cross-sections of unmyelinated axonal profiles less than 300 nm in diameter, adjacent to each other in clusters of more than three per cluster, were counted at 40,000× magnification resulting in a square field of 4 μm × 4 μm and total area of 16 μm^2. Axonal profiles were defined as cell membrane-bound structures encompassing neurotubules, neurofilaments and occasionally a mitochondrion. Three to Five separate areas were used for counts of small axonal profiles in each rat. All structural analyses were performed by an operator blinded to treatment groups.

Statistical analysis of behavioural and electrophysiological data

Data are presented as mean ± the SEM and were analysed with Kruskal–Wallis and Mann–Whitney U tests for non-parametric data. $P < 0.05$ was considered to indicate a significant difference. GraphPad Prism software (GraphPad Software, Inc., La Jolla, CA) was used for all statistical analyses and graphing.

Results

Behavioural studies on mechanical withdrawal threshold

Von Frey tests performed on NEP and CIP model rats on post-surgical days 21–27 immediately prior to electrophysiological experiments revealed decreased mechanical withdrawal thresholds in the ipsilateral limbs relative to sham-injected control rats (Figure 1). In SD rats, withdrawal thresholds were 5.09 ± 0.86 g in NEP model rats (n = 8), 6.10 ± 1.14 g in CIP model rats (n = 8) and 14.44 ± 0.22 g (n = 8) in control rats. Differences between all SD rat groups were significant with $P < 0.0001$ by Kruskal–Wallis testing; and $P < 0.05$ between control versus NEP and control versus CIP groups, while there were no differences between NEP and CIP groups. In CP rats, withdrawal thresholds were significantly different between CIP and control groups at 6.66 ± 0.66 g in CIP model rats (n = 8) and 14.00 ± 0.63 g in control rats (n = 8). Differences between two groups were significant to $P = 0.004$ test by Mann–Whitney U tests.
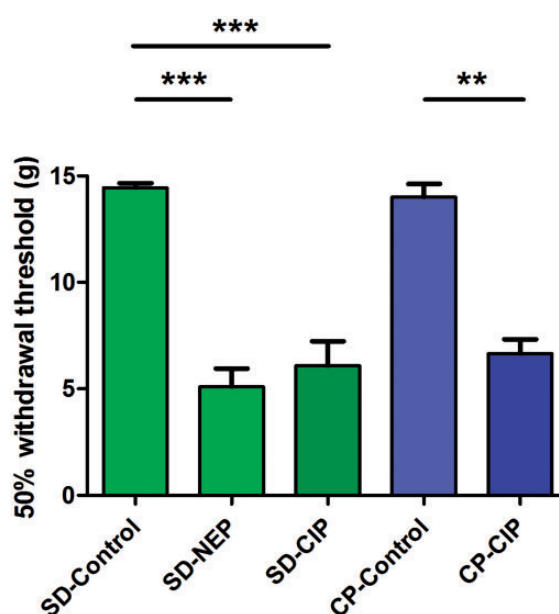

Figure 1. Comparison of 50% mechanical withdrawal threshold. Withdrawal threshold to mechanical stimulation of the plantar surface of the ipsilateral hind paw with von Frey filaments was recorded on the same day (day 21–27) immediately prior to acute electrophysiological experiment. Animals in neuropathic pain (NEP) and cancer-induced pain (CIP) groups demonstrated reduced mechanical withdrawal thresholds relative to control. (SD-control: Naïve control of Sprague-Dawley (SD) rat, SD-NEP: SD rat NEP model, SD-CIP: SD rat breast cancer-induced bone pain (CIP) model, CP-Control: Copenhagen (CP) rat sham-surgery control of CIP model, CP-CIP: CP rat prostate CIP model). Asterisks above the graph indicate significant differences between control and NEP/CIP animals: $**P < 0.01$, $***P < 0.001$. The absence of an asterisk indicates a lack of a statistically significant difference. Kruskal–Wallis tests with post hoc Dunn's multiple comparison tests were used to compare SD rat groups, and Mann–Whitney U testing was used to compare CP rat groups.

Electrophysiological studies on DRG neurons

AP configuration of DRG neurons. The following parameters were analysed from intracellular recording of somatic APs evoked by electrical stimulation of the dorsal root: (1) CV, (2) resting membrane potential (Vm), (3) APA, (4) APdB, (5) APRT, (6) APFT, (7) AHPA and (8) AHP50. Intrasomal recordings in these rats were made from a total of 289 L4 DRG neurons. All neurons included in these results met the criteria for inclusion described above for Aβ-fibre LTM neurons. In female SD rats, a total of 96 CUT neurons were recorded: 31 in control rats, 32 in NEP rats and 33 in CIP rats (12 GF neurons, 10 RA neurons and 9 SA neurons in control rats; 12 GF neurons, 12 RA neurons and 8 SA neurons in NEP rats; and 13 GF neurons, 11 RA neurons and 9 SA neurons in CIP rats). A total of 79 MS neurons were recorded in female SD rats; 26 in control rats, 27 in NEP rats and 26 in CIP rats. In male CP rats, a total of 33

CUT neurons were recorded in control rats and 32 in cancer rats (14 GF neurons, 12 RA neurons and 7 SA neurons in control rats and 13 GF neurons, 12 RA neurons and 7 SA neurons in CIP rats). A total of 24 MS neurons were recorded in control rats and 25 in CIP rats. The various AP parameters of corresponding subclasses of neurons were compared in the 10 groups. All data are shown in scatter plots in Figure 2, illustrating the distributions of various parameters for individual neurons in each neuron type in all rats. All comparisons with statistical analyses are summarized in Table 1.

CV was studied, as it reflects properties of the axon rather than of the soma. Figure 2(a) illustrates the distribution of CV in individual neurons of all neuron types across animal model groups. There were no differences in CV found between groups for all comparisons. In female SD rats, CV of CUT neurons was 16.50 ± 0.60 m/s in control, 14.47 ± 0.92 m/s in NEP and 14.93 ± 0.61 m/s in CIP model rats. CV of MS neurons was 17.99 ± 3.92 m/s in control, 15.51 ± 0.81 m/s in NEP and 18.16 ± 0.84 m/s in CIP. In male CP rats, CUT neuronal CV was 16.20 ± 0.46 m/s in control and 14.98 ± 0.48 m/s in CIP. MS neuronal CV was 16.74 ± 0.66 m/s in control and 14.71 ± 0.75 m/s in CIP.

There were no differences in Vm found between groups for all comparisons (Figure 2(b)). In female SD rats, Vm of CUT neurons was -67.73 ± 1.34 mV in control, -65.21 ± 0.87 mV in NEP and -65.96 ± 1.65 mV in CIP model rats. Vm of MS neurons was -64.52 ± 1.95 mV in control, -61.06 ± 1.09 mV in NEP and -64.19 ± 1.73 mV in CIP model rats. In male CP rats, CUT neuronal Vm was -66.90 ± 1.57 mV in control and -63.54 ± 1.59 mV in CIP, MS neuronal Vm was -65.15 ± 1.43 mV in control and -62.81 ± 1.55 mV in CIP.

The APA of Aβ-fibre neurons was decreased in all groups of NEP and CIP model rats relative to their respective controls (Figure 2(c)). In female SD rats, APA of CUT neurons showed decreased trend APA ($P = 0.061$), which was 65.03 ± 1.86 mV in control, 59.41 ± 1.20 mV in NEP and 59.95 ± 1.54 mV in CIP model rats. MS neurons also showed decreased trend APA ($P = 0.061$), which was 59.39 ± 1.28 mV in CIP, 56.13 ± 1.25 mV in NEP and 57.15 ± 1.87 mV in CIP. In male CP rats, both CUT neurons and MS neurons showed significantly decreased APA. CUT neuronal APA was 67.27 ± 2.55 mV in control and 60.70 ± 2.55 mV in CIP ($P = 0.032$), MS neuronal APA was 61.25 ± 3.14 mV in control and 55.49 ± 1.41 mV in CIP ($P = 0.022$).

Aβ-fibre neurons in NEP and CIP model groups also exhibited longer APdB relative to their respective controls (Figure 2(d)). In female SD rats, CUT neurons in NEP and CIP groups showed significantly longer APdB (control: 1.25 ± 0.05 ms, NEP: 1.48 ± 0.06 ms, CIP: 1.58 ± 0.10 ms; $P = 0.015$). In SD rats, MS neurons showed

no differences between groups (control: 0.92 ± 0.19 ms vs. NEP: 1.15 ± 0.08 ms, CIP: 1.08 ± 0.05 ms; $P = 0.133$). In male CP rats, both CUT and MS neurons exhibited longer APdB in CIP rats – CUT neuronal APdB (control: 1.34 ± 0.02 ms vs. CIP, 1.55 ± 0.06 ms; $P = 0.019$), MS neuronal APdB (control: 1.03 ± 0.03 ms vs. CIP: 1.20 ± 0.06 ms; $P = 0.016$).

Both NEP and CIP model rats exhibited significant differences in APRT relative to controls (Figure 2(e)). In female SD rats, CUT neurons in NEP and CIP groups showed longer APRT duration (control: 0.49 ± 0.02 ms; NEP: 0.56 ± 0.02 ms; CIP: 0.57 ± 0.03 ms; $P = 0.047$). There were no differences in APRT of MS neurons between groups of SD rats (control: 0.44 ± 0.02 ms, NEP: 0.51 ± 0.02 ms, CIP: 0.47 ± 0.02 ms; $P = 0.226$). In male CP rats, both CUT and MS neurons showed longer APRT in CIP rats relative to control. CUT neuronal APRT (control: 0.46 ± 0.01 ms vs. CIP: 0.52 ± 0.02 ms; $P = 0.022$), MS neuronal APRT (control: 0.42 ± 0.02 ms vs. CIP: 0.49 ± 0.01 ms; $P = 0.028$).

There were no differences in APFT found between groups for all comparisons (Figure 2(f)). In female SD rats, APFT of CUT was 0.77 ± 0.04 ms in control, 0.91 ± 0.06 ms in NEP and 1.01 ± 0.08 ms in CIP model rats. APRT of MS was 0.49 ± 0.04 ms in control, 0.61 ± 0.07 ms in NEP and 0.61 ± 0.05 ms in CIP. In male CP rats, CUT neuronal APFT was 0.88 ± 0.03 ms in control and 0.83 ± 0.06 ms in CIP, MS neuronal APFT was 0.61 ± 0.03 ms in control and 0.71 ± 0.03 ms in CIP.

There were also no differences in AHPA between groups for all comparisons (Figure 2(g)). In female SD rats, AHPA of CUT was 7.24 ± 0.09 mV in control, 5.57 ± 0.54 mV in NEP and 5.08 ± 0.69 mV in CIP. AHPA of MS was 6.76 ± 0.75 mV in control, 7.30 ± 0.72 mV in NEP and 6.82 ± 0.92 mV in CIP model rats. In male CP rats, CUT neuronal AHPA was 6.76 ± 0.39 mV in control and 6.21 ± 0.53 mV in CIP. MS neuronal AHPA was 6.69 ± 0.39 mV in control and 6.94 ± 0.43 mV in CIP.

Finally, AHP50 was also not different between groups in all comparisons (Figure 2(h)). In female SD rats, AHP50 of CUT was 6.28 ± 1.24 ms in control, 6.04 ± 1.05 ms in NEP and 5.07 ± 0.95 ms in CIP. MS neuronal AHP50 was 1.66 ± 0.14 ms in control, 2.27 ± 0.24 ms in NEP and 2.04 ± 0.15 ms in CIP. In male CP rats, CUT neuronal AHP50 was 5.91 ± 0.41 ms in control and 5.50 ± 0.45 ms in CIP, MS neuronal AHP50 was 2.71 ± 0.30 ms in control and 3.19 ± 0.36 mV in CIP.

Excitability of the soma measured by responses to injection of depolarizing current. AP responses to intracellular depolarizing current injection were recorded to determine whether there were differences in soma excitability in the NEP and CIP models. Figure 3(a) illustrates the threshold currents that elicited APs in the different model groups of SD rats. In SD rats, CUT neurons
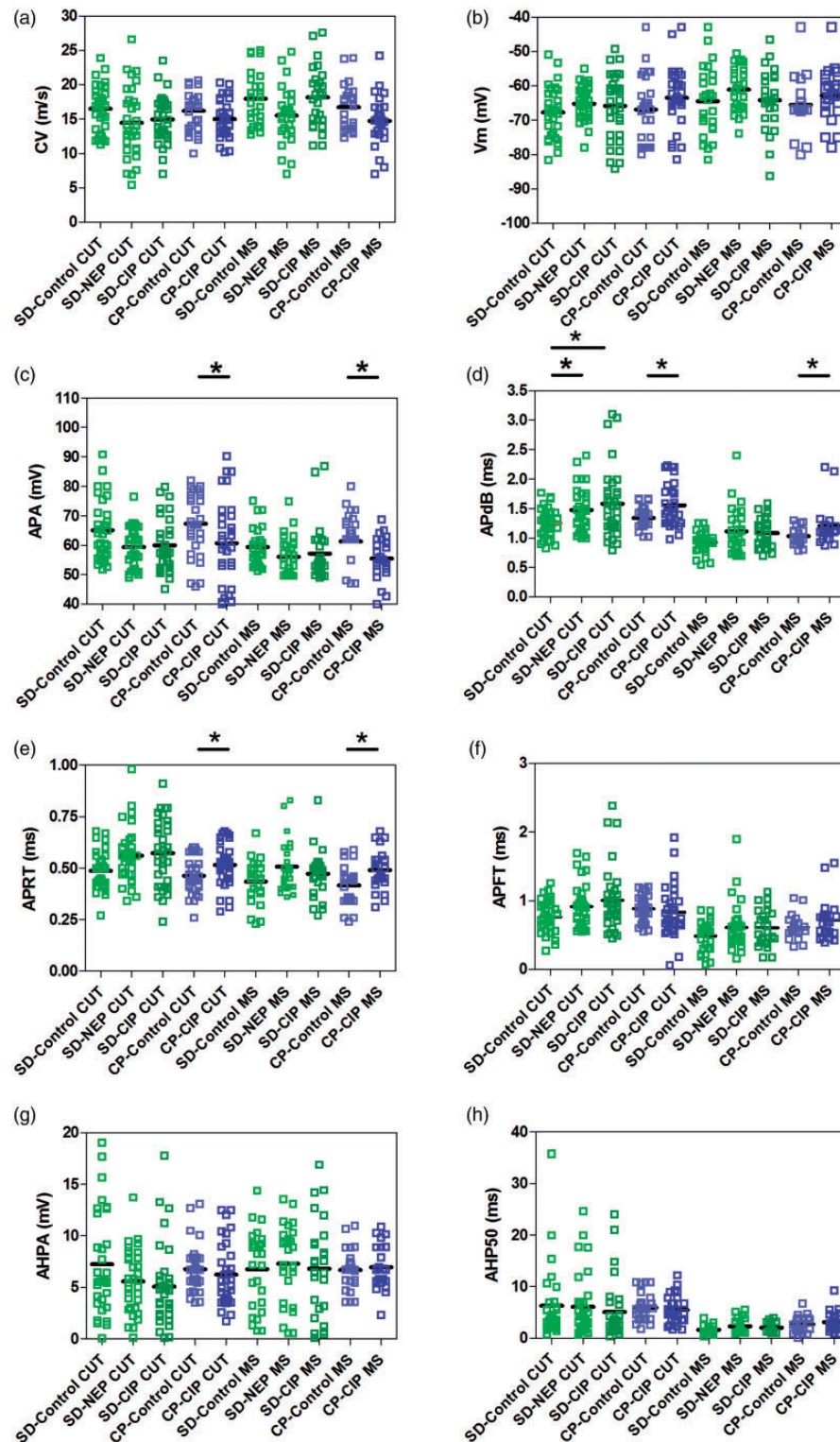
Figure 2. Action potential configuration changes in DRG neurons. Scatter plots show the distribution of action potential variables generated by stimulation of the dorsal root with the median (horizontal line) superimposed in nonnociceptive Aβ-fibre LTM neurons. Panels are as follows: (a) conduction velocity (CV); (b) resting membrane potential (Vm); (c) action potential amplitude (APA); (d) action potential duration at base (APdB); (e) action potential rise time (APRT); (f) action potential fall time (APFT); (g) afterhyperpolarization amplitude below Vm (AHPA); (h) afterhyperpolarization duration to 50% recovery (AHP50). Cutaneous neurons (CUT) including Aβ-fibre LTM GF, RA and SA neurons are indicated by red. Muscle spindle neurons (MS) are indicated by green. *$P < 0.05$, **$P < 0.01$; Kruskal–Wallis tests with post hoc Dunn's multiple comparison tests were used to compare SD rat groups, and Mann–Whitney U testing was used to compare CP rat groups. Other abbreviations are as indicated in Figure 1.

Table 1. Comparison of AP configuration of DRG neurons between control, neuropathic, and CIP rats.

	CV	Vm	APA	APdB	APRT	APFT	AHP	AHP50
Cut neuron type								
SD-control (n = 31) vs. SD-NEP (n = 32)	No	No	No	Yes	No	No	No	No
SD-control (n = 31) vs. SD-CIP (n = 33)	No	No	No	Yes	No	No	No	No
SD-NEP (n = 32) vs. SD-CIP (n = 33)	No	No	No	No	No	No	No	No
P value	0.116	0.305	0.061	0.015	0.047	0.094	0.156	0.462
CP-control (n = 33) vs. CP-CIP (n = 32)	No	No	Yes	Yes	Yes	No	No	No
P value	0.099	0.063	0.032	0.019	0.022	0.178	0.174	0.321
MS neuron type								
SD-control (n = 26) vs. SD-NEP (n = 27)	No	No	No	No	No	No	No	No
SD-control (n = 26) vs. SD-CIP (n = 26)	No	No	No	No	No	No	No	No
SD-NEP (n = 27) vs. SD-CIP (n = 26)	No	No	No	No	No	No	No	No
P value	0.077	0.23	0.061	0.133	0.226	0.348	0.753	0.127
CP-control (n = 24) vs. CP-CIP (n = 25)	No	No	Yes	Yes	Yes	No	No	No
P value	0.082	0.067	0.022	0.016	0.028	0.246	0.704	0.478

Note: The numbers of each neuron type are reported in the table. In SD rats, Kruskal–Wallis tests with post hoc Dunn's multiple comparison tests were performed for comparing CUT and MS neurons individually among Control, NEP and CIP groups. Results of Dunn's multiple comparison tests are reported in the table for pairwise comparisons between groups, and P values derived from Kruskal–Wallis testing are shown below each section. In CP rats, Mann-Whitney U tests were performed for comparing CUT and MS neurons individually between control and CIP model rats. *P*-values are shown below each section, $P < 0.05$ was considered to indicate a significant difference between groups. *$P < 0.05$, **$P < 0.01$, ***$P < 0.001$. AP: action potential; MS: muscle spindle; CP: Copenhagen rats; NEP: neuropathic pain; CIP: cancer-induced pain; CV: conduction velocity; Vm: resting membrane potential; APA: action potential amplitude; APdB: action potential duration at base; APRT: action potential rise time; APFT: action potential fall time; AHP: afterhyperpolarization; AHP50: afterhyperpolarization duration at 50% recovery.

showed no differences in stimulation threshold between groups (control: 1.14 ± 0.06 nA, NEP: 0.87 ± 0.15 nA, CIP: 0.86 ± 0.15 nA; $P = 0.279$). There was a significant decrease in the threshold necessary to elicit an AP in MS neuron in SD NEP and CIP model rats relative to control (control: 0.60 ± 0.13 nA, NEP: 0.22 ± 0.03 nA, CIP: 0.22 ± 0.07 nA; $P = 0.011$).

Figure 3(b) shows the number of APs elicited in response to 2 nA current injections. Similarly, in SD rats, CUT neurons showed no differences in the number of elicited APs between groups (control: 0.67 ± 0.33, NEP: 1.17 ± 0.34, CIP: 0.83 ± 0.11; $P = 0.169$; n = 12 neurons/group). MS neurons showed an increased number of elicited APs in response to a 2 nA stimulation in SD NEP and CIP model rats relative to control (control: 3.13 ± 0.63, NEP: 5.88 ± 0.55, CIP: 5.25 ± 0.57; $P = 0.009$; n = 10 neurons/group). Figure 3 (c) to (e) shows typical discharge patterns elicited in MS neurons by 2 nA current pulses with a duration 100 ms. In this figure, control rats show 6–8 Aps, while NEP model rats show 17 APs and CIP model rats show 16 APs in response to the same current pulse injection, which was the maximum number of APs observed using 2 nA current pluses. These data in CP rats were published previously.[25]

Excitability of the dorsal root measured by responses to dorsal root stimulation. Dorsal root excitability was determined as the chronaxie (threshold-duration curve), which was derived by determining the minimum current applied to

the dorsal root to evoke a soma AP with pulse durations of 0.2, 1, 2, 4 and 6 ms. In SD rats, there were no differences between groups in CUT neuron thresholds for all pulse durations (Figure 3(a)). MS neurons (Figure 3(b)) showed significantly lower current intensity threshold with 0.2 ms stimulation in NEP rats (control: 0.45 ± 0.07 mA, NEP: 0.21 ± 0.02 mA, CIP: 0.25 ± 0.03 mA; $P = 0.007$ control vs. NEP; $P = 0.026$ control vs. CIP). There were no differences in MS neuron threshold between groups for all other pulse durations.

Figure 4(c) to (e) shows typical discharge patterns elicited in sensory neurons by 0.5 mA current pulses with a duration of 0.2 ms. In this figure, control rats showed 1 AP, while NEP and CIP rats showed 2–5 APs in response to the same current pulse injection.

Ultrastructural study of the lumbar spinal cord

Results of the light microscopic and ultrastructural analyses of the entire section of the spinal cord at L4 from four groups of rats – CP CIP-model rats (n = 4), CP sham control t (n = 1), SD NEP rats (n = 3) and SD sham control rat (n = 1)– are shown in Figure 5. Within the bundles of myelinated axons in laminae IV and V of the grey matter detailed in control animals in Figure 5(a) and (b), there were stacks of numerous small axonal profiles. The individual small axonal profiles measured less than 300 nm in diameter, tightly adhered to each other and encompassed microtubules, neurofilaments and occasionally a mitochondrion. Three to five
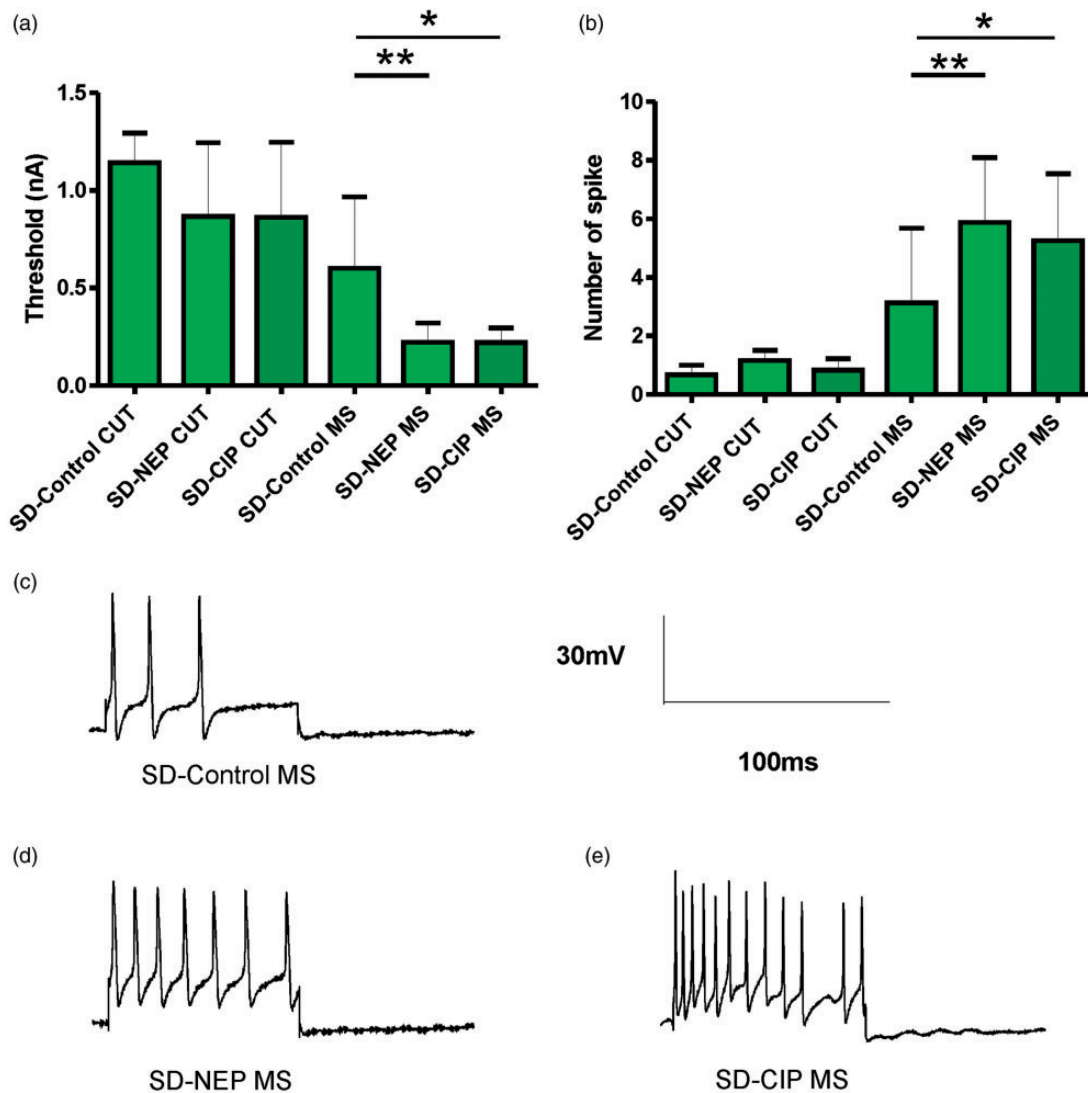
Figure 3. Excitability changes of DRG neurons by soma stimulation. (a) The current threshold was defined as the minimum current required to evoke an AP by intracellular current injection (20 ms) at the soma. Excitability of the DRG somata was significantly increased in NEP and CIP model rats, as indicated by the decreased activation threshold in CUT and MS neurons. (b) A comparison of the repetitive discharge characteristic of DRG cells produced by intracellular current injection. Columns indicate the number of APs evoked by 2 nA, 100 ms intracellular depolarizing current injection in different groups. MS neurons in the NEP and CIP models showed a significantly increased number of APs. (c-e) Representative examples of raw recordings to demonstrate the greater number of APs evoked by intracellular current injection in MS neurons in control (c) versus NEP (d) and CIP model rats (e), arrows indicate the time of stimulation. $*P < 0.05$, $**P < 0.01$; Kruskal–Wallis tests with post hoc Dunn's multiple comparison tests were used to compare SD rat groups. Other abbreviations are as indicated in Figure 1.

different imaged fields at $40,000\times$ magnification from each rat were used for counts of small axonal profiles. Mean counts of these structures on the side ipsilateral to the site of model induction on the right hind limb are 32.06 ± 26.59 (n = 19 fields) in CP-CIP rats and 31.01 ± 14.89 (n = 10 fields) in SD-NEP rats (Figure 5(d) and (j)). However, numbers of such small axonal profiles on the contralateral side of these same rats (Figure 5(e) and (k)) and in ipsilateral and contralateral sides of CP-control and SD-control (Figure 5(g), (h), (m) and (n)) were fewer, with grouped mean counts of 15.26 ± 6.89

(n = 19 fields) for CP rats and 15.20 ± 7.40 (n = 5 fields) for SD rats. Counts are listed as mean $\pm$ SEM. The comparison in CP rats between CIP model and their control ($P = 0.019$) and in SD rats between NEP model and their control ($P = 0.042$) are both significant as compared by Mann–Whitney U testing.

Discussion

This study describes similar changes in Aβ DRG neurons and similar abnormal increase in axonal
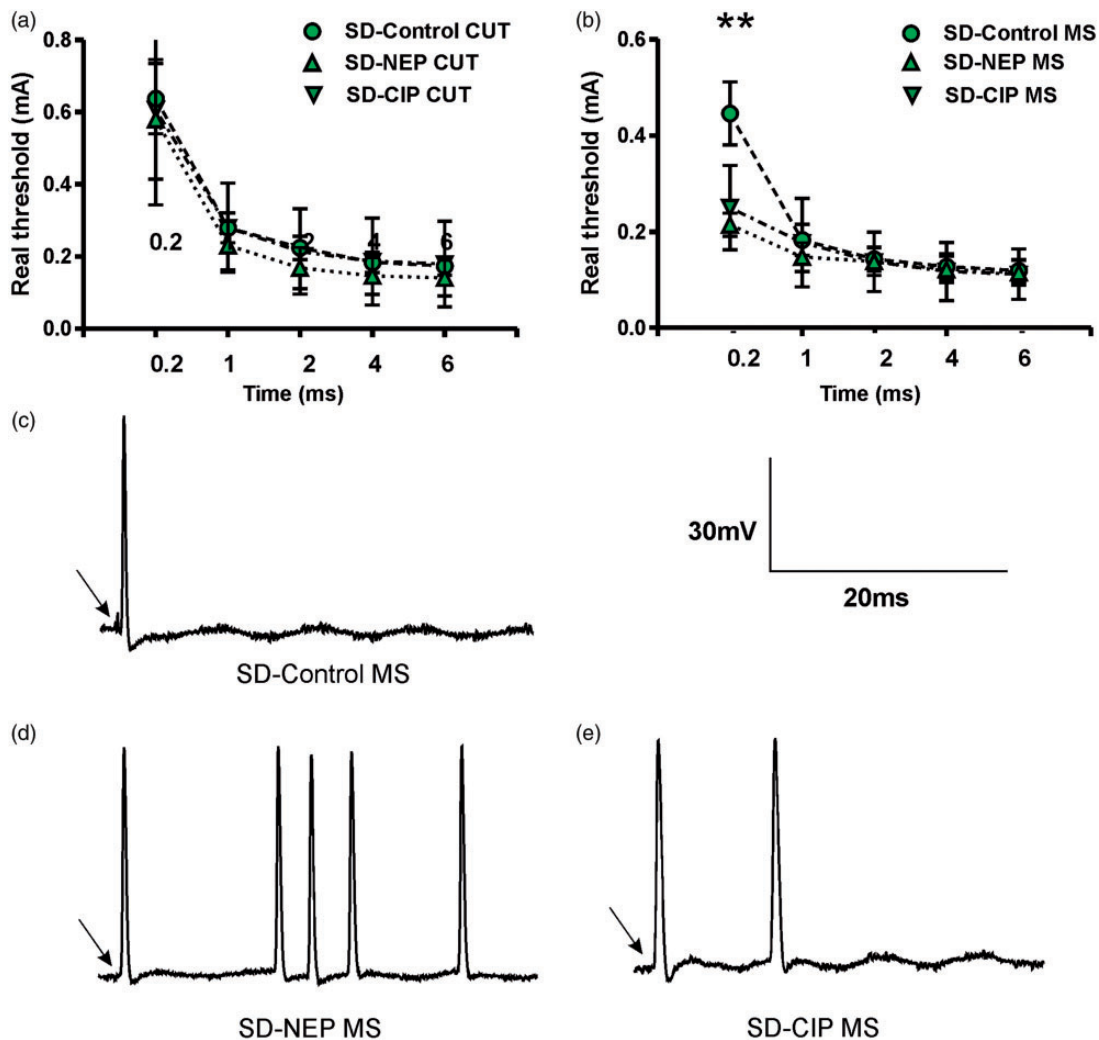
Figure 4. Excitability changes of DRG neurons by dorsal root stimulation. (a-b) Dorsal root current threshold was defined by the chronaxie curve (threshold-duration), which was determined as the minimum stimulus current to the dorsal root sufficient to evoke a soma AP with pulses of 0.2, 1, 2, 4 and 6 ms duration. A reduction in the rheobase in DRG neurons is shown in the NEP and CIP models. MS (B) neurons showed significant reduction with a 0.2 ms pulse. (c–e). Representative examples of MS neurons raw recordings to demonstrate the greater number of APs evoked by dorsal root stimulation in control (c) versus NEP model (d) and CIP model rats (e). *$P < 0.05$, **$P < 0.01$; Kruskal–Wallis tests with post hoc Dunn's multiple comparison tests were used to compare SD rat groups. Other abbreviations are as indicated in Figure 1.

plasticity which we interpret as sprouting in the lumbar spinal cord in rat models of CIP and peripheral nerve injury-induced NEP. The similarity of these models suggests that nociceptive scores in the CIP models may have been partly due to pathological changes in sensory neurons indicating that cancer pain includes structural and functional neuropathic plasticity. Further, the changes in normally non-nociceptive Aβ-fibre sensory neurons and the abnormal distribution of primary sensory nerve terminals in the spinal cord in both models suggest that these neurons play a specific role in the aetiology of bone cancer pain.

Correlation of tactile hypersensitivity in CIP and NEP models

NEP can be spontaneous (stimulus-independent) and evoked (stimulus-dependent) with exaggerated intensity or distorted quality evoking abnormal sensations, such as allodynia or hyperalgesia, described as uncommon tactile and thermal sensations.[26,27] Several studies have shown that implantation of tumour cells into hind leg bone produces behavioural signs of neuropathic ongoing and evoked pain,[9,28,29] as well as increased responsiveness to mechanical,[9,28–31] heat[28] and cold stimuli[7,10,29] applied to the ipsilateral hind paw. Previous results
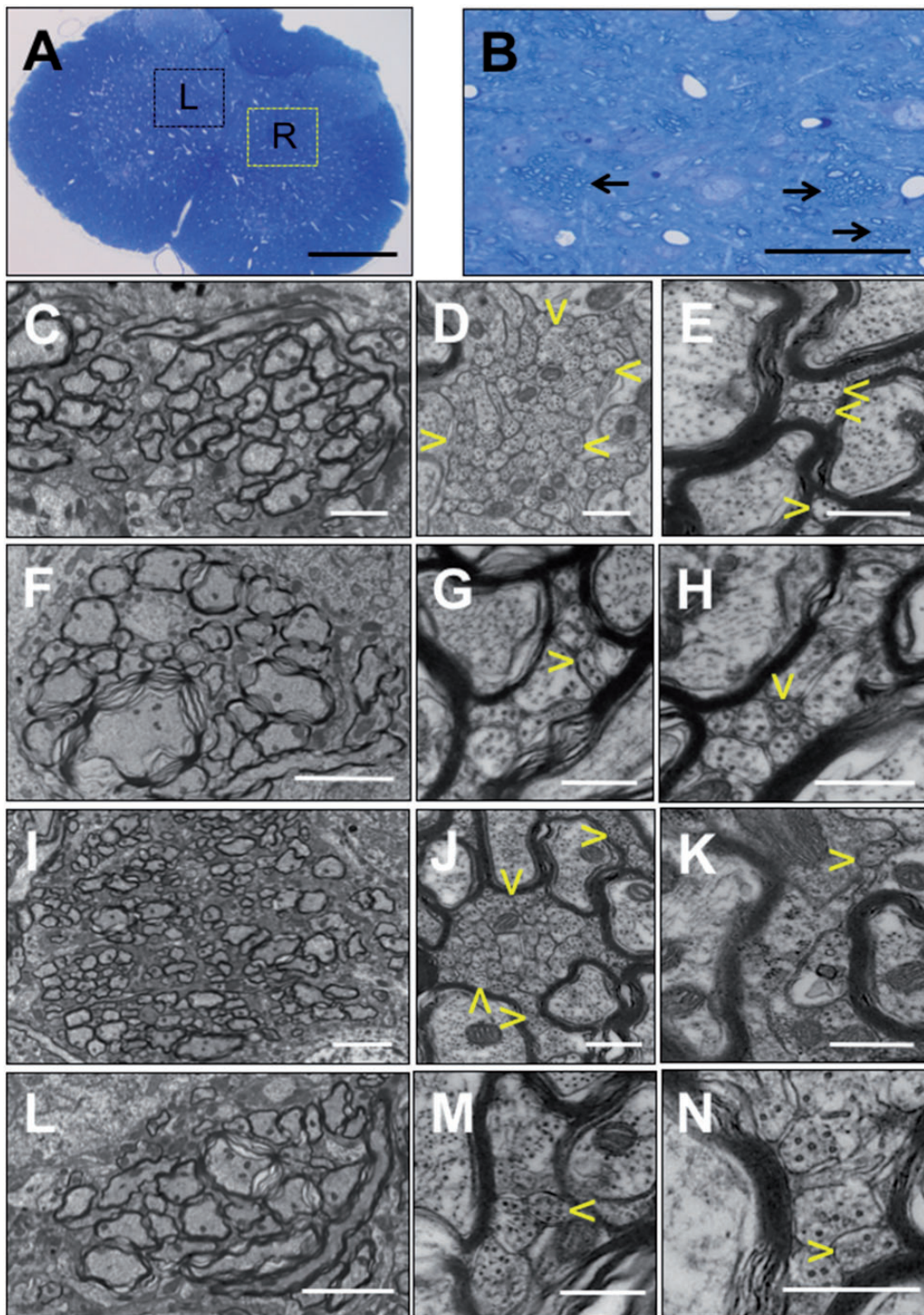
Figure 5. Morphologic analysis of the induction of axonal plasticity in the dorsal horn of the rat lumbar spinal cord. (a). A cross-section of the lumbar (L4) spinal cord of a Copenhagen sham-control rat. In the lamina IV and V of the gray matter, there are multiple bundles of myelinated axons within the boxed areas of the ipsilateral right (R) and contralateral left (L) spinal cord. Detail of myelinated bundles is further presented in (b) in a magnified area indicated in the yellow box (R), there are bundles of myelinated axons indicated by arrows. In (c–e), the ipsilateral area of the CIP model, a bundle of myelinated axons (c) has areas of large aggregation of small axonal profiles (delineated by yellow arrowheads in (d)), which are <300 nm in diameter. Similar bundles of myelinated axons in the contralateral gray

(continued)

obtained in mouse, rat and human patients show that CIP can induce hypersensitivity of the nearby skin.[32–41] In the present study, both male and female CIP and NEP rats demonstrated behavioural evidence suggesting a decreased threshold for mechanical stimulation in the ipsilateral limbs compared to control rats. Furthermore, the hind leg withdrawal response was often exaggerated and accompanied by licking of the paw. This tactile hypersensitivity suggests behavioural neuropathic symptoms in these NEP and CIP models.

Correlation of Aβ-type LTM neuron plasticity in CIP and NEP models

It has become evident that peripheral NEP is characterized by ectopic activity generated in both damaged as well as neighboring intact/surviving primary sensory neuron fibres. Previous studies have shown that ectopic activity may arise from the DRG soma, along axons, or from peripheral nerve terminals[26,42–46] and that prolonged responses to sensory inputs of dorsal horn neurons in neuropathic rat models are reduced by local anaesthetic application to the peripheral sensory nerve.[15,16] As similar results have been obtained in several animal models of peripheral neuropathy,[12,15,16,18,26,27] we compared the electrophysiological and morphological characteristics of sensory neurons in animal models of CIP and of NEP in an effort to identify mechanisms of cancer-induced NEP.

AP configuration, CV and peripheral activation thresholds of Aβ-fibre LTM DRG neurons were systemically evaluated in this study, as each of these parameters might reflect changed electrophysiological properties in various parts of the primary sensory neuron, such as the soma, the axon and the receptive field. The observed phenotype changes of peripheral neurons in both models are associated with Aβ-fibre LTMs.

It is widely believed that afferent C-fibre input is a necessary condition for the induction and maintenance of central sensitization. However, none of the C-fibre neurons in our previous study on the same NEP model showed any differences in electrophysiological properties.[12] Perhaps most importantly, no C-fibre HTM neurons showed any changes in mechanical sensitivity when tested with von Frey filaments.[12] Thus, although our studies have found differences in the electrophysiological properties of functionally identified nociceptive sensory neurons in the rat prostate CIP model,[11] the present results indicating the involvement of normally non-nociceptive Aβ-fibre LTM neuron plasticity provide evidence for a possible role for Aβ-fibre LTMs in the generation or maintenance of the neuropathic component of CIP.

Significance of abnormal sprouting in the lumbar spinal cord in CIP and NEP models

The hypothesis that severe chronic pain is a pathologic process that is processed in the CNS and is expected to be associated with discernible structural changes such as abnormal axonal plasticity evidenced as sprouting is supported by the results of ultrastructural analysis and by the results of quantitation of small axonal profiles in the L4 spinal cord in this study.

Several studies have demonstrated that animal models of chronic pain have significant pathological changes in the CNS that contribute to the generation and maintenance of pain.[47,48] In models of both CIP and NEP, pursuant to peripheral changes, secondary neurons in the spinal cord exhibit increased spontaneous activity and enhanced responsiveness to three modes of noxious stimulation: heat, cold and mechanical stimuli.[16,17,49] It has been reported that in CIP mice there are simultaneous changes including concurrent modification in dynorphin, galanin, ATF3, astrocytes (GFAP), microglia, c-Fos expression and substance-P receptor internalization in the spinal cord.[35] Peripheral nerve injury has also been shown to result in axonal plasticity of myelinated afferents, primarily Aβ fibres in the ipsilateral dorsal horn following retrograde tracing with horseradish peroxidase.[50–54]

For abundant sprouting to occur in the CNS of a mature animal, the absence of myelin sheaths is required such as in the optic nerve[55] and the spinal cord[56] of the Long Evans Shaker (LES) rat. A limited injury to the CNS caused formation of stacks of numerous sprouts in

Figure 5. Continued.
matter contain only rare, individual axonal profiles <300 nm (yellow arrowheads in (e)). In the CP sham-surgery control model rat (f–h), the myelinated axon bundles of the dorsal horn (f) have low numbers of small axonal profiles in the ipsilateral (g) and contralateral (h) horns. In SD-NEP model rats (i–k), the ipsilateral dorsal horn that shows a bundle of cross-sections of myelinated axons (i) has aggregations of numerous profiles of axonal sprouts (delineated by yellow arrowheads in (h)) which are smaller than 300 nm in diameter. In the contralateral dorsal horn, similar bundles have only rare individual axonal profiles <300 nm (arrowhead in (k)) intermixed with large unmyelinated axonal profiles. In SD-control rats (L-N), bundles of cross-sections of myelinated axons contain rare axonal profiles <300 nm that are intermixed with larger unmyelinated profiles in both dorsal horns (m and n). (a and b) Toluidine blue. (c to n) TEM. Size of bars: (a) 500 μm, (b) 50 μm, (i and l) 4 μm, (c and f) 2 μm, (d, e, g, h, j, k, m and n) 500 nm. Samples were analysed from Copenhagen CIP-model rats (n = 4), Copenhagen sham control rat (n = 1), SD NEP rats (n = 3) and SD sham control rat (n = 1). Other abbreviations are as indicated in Figure 1.

the spinal cord of the LES rat,[57] similar to the stacks of abnormal small axonal profiles observed in this study. In the environment of the myelinated CNS, including the bundles of myelinated axons in laminae IV and V, axonal plasticity is constitutively inhibited unless a pathologic process such as that induced by severe pain in CIP and NEP rat models is initiated and sustained. In the present study, we present ultrastructural and quantitative evidence of axonal sprouting in the bundles of myelinated fibres in laminae IV and V in CIP and NEP rat models. Previous studies have shown that myelinated afferents sprout into Lamine II of the L3-5 dorsal horn following chronic constriction nerve injury in rats.[52] We intend to perform further investigation to identify if the abnormal sprouting observed in CIP and NEP models in the current study is from $A\beta$-fibre LTM plasticity or other fibre types. $A\beta$-fibre neurons terminate in the deeper layers of the dorsal horn, primarily in laminae III, IV and V where they terminate on wide dynamic range (WDR) neurons. Notably, a previous study on the same NEP model that demonstrated ectopic activity recorded from WDR dorsal horn neurons was mediated by myelinated afferents.[17] Thus, this abnormal phenotypic change of the deep dorsal horn population accompanied by a WDR hyperexcitability to mechanical stimuli appears to correlate with the development of behavioural neuropathic signs in these CIP and NEP models. This suggests that an ongoing state of central sensitization occurs in both pain models including involvement of axonal sprouting.

Possible mechanism of $A\beta$-type LTM neuron plasticity in CIP models

As discussed above, we found that $A\beta$-type LTM neurons ending in paw skin and muscle of the ipsilateral limb of CIP and NEP model animals showed plastic activity at the DRG. In addition, we have observed structural axonal plasticity of fibres within bundles of myelinated axons in dorsal horn laminae IV and V. However, the mechanisms that drive this plasticity are not well understood.

Altered AP configuration and enhanced excitability of DRG neurons may be due to membrane remodeling, thus altering the intrinsic electrogenic properties of the neuronal membrane in those neuron types exhibiting changes.[22] There are three major ion channels: Na^+, Ca^{2+} and K^+ that play major roles in determining the electrogenic properties of neurons. Alterations in expression, cellular localization, distribution or the activation/kinetics of each of these ion channel types might lead to the observed changes in AP configuration and excitability in NEP and CIP rats. Explanations for the mechanisms underlying these changes in membrane channel expression are not yet apparent.

Periosteum and mineralized bone have been shown to be innervated by a limited population of sensory neurons, including nociceptive C- and $A\delta$-fibres but largely without the myelinated non-nociceptive $A\beta$ sensory innervation characteristic of muscle and skin.[58] However, animal models of cancer implanted in the bone demonstrate neuropathological changes beyond constitutively bone-innervating fibres themselves. Preclinical studies on CIP rats with significant osteolytic degradation of the cortical and trabecular bone and extensive tumour replacement of marrow has also demonstrated significant neuronal, glial and inflammatory changes in the CNS.[35] Guedon et al. describe three possible mechanisms that drive bone cancer-induced hypersensitivity of the skin, including DRG dysfunction,[8] spinal cord pathology[33,35,59] and central sensitization involving modulation of signals to and from the brain.[10,59–62] These mechanisms in turn may result in changes to the descending modulation and ascending facilitation of non-noxious sensory signalling and may not only involve skeletal dysfunction and accompanying skeletal pain but may also affect normally non-noxious skin sensory dysfunction and pain.[32]

The patterns of the changes observed in $A\beta$-LTM sensory neurons in the DRG and the abnormal axonal sprouting in the lumbar spinal dorsal horn are similar in rat models of CIP and NEP. These findings add to the body of evidence that the cancer pain state includes features of NEP that may contribute to the peripheral and central sensitization and tactile hypersensitivity characteristic in models of CIP.

Declaration of Conflicting Interests

Funding

References

1. Foley KM. Controlling cancer pain. *Hosp Pract (1995)* 2000; 35: 101–108, 111–112.
2. Mercadante S. Malignant bone pain: pathophysiology and treatment. *Pain* 1997; 69: 1–18.
3. Currie GL, Delaney A, Bennett MI, Dickenson AH, Egan KJ, Vesterinen HM, Sena ES, Macleod MR, Colvin LA and Fallon MT. Animal models of bone cancer pain: systematic review and meta-analyses. *Pain* 2013; 154: 917–926.
4. Slosky LM, Largent-Milnes TM and Vanderah TW. Use of animal models in understanding cancer-induced bone pain. *Cancer Growth Metastasis* 2015; 8: 47–62.
5. Clohisy DR and Mantyh PW. Bone cancer pain. *Clin Orthop* 2003; 415: S279–S288.
6. Colvin L and Fallon M. Challenges in cancer pain management–bone pain. *Eur J Cancer Oxf Cancer* 2008; 44: 1083–1090.
7. Donovan-Rodriguez T, Dickenson AH and Urch CE. Superficial dorsal horn neuronal responses and the emergence of behavioural hyperalgesia in a rat model of cancer-induced bone pain. *Neurosci Lett* 2004; 360: 29–32.
8. Peters CM, Ghilardi JR, Keyser CP, Kubota K, Lindsay TH, Luger NM, Mach DB, Schwei MJ, Sevcik MA and Mantyh PW. Tumor-induced injury of primary afferent sensory nerve fibres in bone cancer pain. *Exp Neurol* 2005; 193: 85–100.
9. Schwei MJ, Honore P, Rogers SD, Salak-Johnson JL, Finke MP, Ramnaraine ML, Clohisy DR and Mantyh PW. Neurochemical and cellular reorganization of the spinal cord in a murine model of bone cancer pain. *J Neurosci* 1999; 19: 10886–10897.
10. Urch CE, Donovan-Rodriguez T and Dickenson AH. Alterations in dorsal horn neurones in a rat model of cancer-induced bone pain. *Pain* 2003; 106: 347–356.
11. Zhu YF, Ungard R, Seidlitz E, Zacal N, Huizinga J, Henry JL, and Singh G. Differences in electrophysiological properties of functionally identified nociceptive sensory neurons in an animal model of cancer-induced bone pain. *Mol Pain* 2016; 12: 1–14.
12. Zhu YF, Wu Q and Henry JL. Changes in functional properties of A-type but not C-type sensory neurons in vivo in a rat model of peripheral neuropathy. *J Pain Res* 2012; 5: 175–192.
13. De Ciantis PD, Yashpal K, Henry J and Singh G. Characterization of a rat model of metastatic prostate cancer bone pain. *J Pain Res* 2010; 3: 213–221.
14. Mosconi T and Kruger L. Fixed-diameter polyethylene cuffs applied to the rat sciatic nerve induce a painful neuropathy: ultrastructural morphometric analysis of axonal alterations. *Pain*. 1996; 64: 37–57.
15. Pitcher GM and Henry JL. Second phase of formalin-induced excitation of spinal dorsal horn neurons in spinalized rats is reversed by sciatic nerve block. *Eur J Neurosci* 2002; 15: 1509–1515.
16. Pitcher GM and Henry JL. Nociceptive response to innocuous mechanical stimulation is mediated via myelinated afferents and NK-1 receptor activation in a rat model of neuropathic pain. *Exp Neurol* 2004; 186: 173–197.
17. Pitcher GM and Henry JL. Governing role of primary afferent drive in increased excitation of spinal nociceptive neurons in a model of sciatic neuropathy. *Exp Neurol* 2008; 214: 219–228.
18. Zhu YF and Henry JL. Excitability of Aβ sensory neurons is altered in an animal model of peripheral neuropathy. *BMC Neurosci* 2012; 13: 15.
19. Wu Q and Henry JL. Changes in Abeta non-nociceptive primary sensory neurons in a rat model of osteoarthritis pain. *Mol Pain* 2010; 6: 37.
20. Dixon WJ. Efficient analysis of experimental observations. *Annu Rev Pharmacol Toxicol* 1980; 20: 441–462.
21. Chaplan SR, Bach FW, Pogrel JW, Chung JM and Yaksh TL. Quantitative assessment of tactile allodynia in the rat paw. *J Neurosci Methods* 1994; 53: 55–63.
22. Djouhri L, Bleazard L and Lawson SN. Association of somatic action potential shape with sensory receptive properties in guinea-pig dorsal root ganglion neurones. *J Physiol* 1998; 513: 857–872.
23. Lawson SN, Crepps BA and Perl ER. Relationship of substance P to afferent characteristics of dorsal root ganglion neurones in guinea-pig. *J Physiol* 1997; 505: 177–191.
24. Kwiecien JM, Blanco M, Fox JG, Delaney KH and Fletch AL. Neuropathology of bouncer Long Evans, a novel dysmyelinated rat. *Comp Med* 2000; 50: 503–510.
25. Zhu YF, Ungard R, Zacal N, et al. Rat model of cancer-induced bone pain. *Pain Reports* 2017; 2: e603.
26. Campbell JN and Meyer RA. Mechanisms of neuropathic pain. *Neuron* 2006; 52: 77–92.
27. Devor M. Ectopic discharge in Abeta afferents as a source of neuropathic pain. *Exp Brain Res* 2009; 196: 115–128.
28. Menéndez L, Lastra A, Fresno MF, Llames S, Meana A, Hidalgo A and Baamonde A. Initial thermal heat hypoalgesia and delayed hyperalgesia in a murine model of bone cancer pain. *Brain Res* 2003; 969: 102–109.
29. Wacnik PW, Kehl LJ, Trempe TM, Ramnaraine ML, Beitz AJ and Wilcox GL. Tumour implantation in mouse humerus evokes movement-related hyperalgesia exceeding that evoked by intramuscular carrageenan. *Pain* 2003; 101: 175–186.
30. Luger NM, Mach DB, Sevcik MA and Mantyh PW. Bone cancer pain: from model to mechanism to therapy. *J Pain Symptom Manage* 2005; 29: S32–S46.

31. Medhurst SJ, Walker K, Bowes M, Kidd BL, Glatt M, Muller M, Hattenberger M, Vaxelaire J, O'Reilly T, Wotherspoon G, Winter J, Green J and Urban L. A rat model of bone cancer pain. *Pain* 2002; 96: 129–140.

32. Guedon J-MG, Longo G, Majuta LA, Thomspon ML, Fealk MN and Mantyh PW. Dissociation between the relief of skeletal pain behaviours and skin hypersensitivity in a model of bone cancer pain. *Pain* 2016; 157: 1239–1247.

33. Hald A, Hansen RR, Thomsen MW, Ding M, Croucher PI, Gallagher O, Ebetino FH, Kassem M and Heegaard A-M. Cancer-induced bone loss and associated pain-related behaviour is reduced by risedronate but not its phosphonocarboxylate analog NE-10790. *Int J Cancer* 2009; 125: 1177–1185.

34. Hald A, Nedergaard S, Hansen RR, Ding M and Heegaard A-M. Differential activation of spinal cord glial cells in murine models of neuropathic and cancer pain. *Eur J Pain Lond Pain* 2009; 13: 138–145.

35. Honore P and Mantyh PW. Bone cancer pain: from mechanism to model to therapy. *Pain Med Malden Med* 2000; 1: 303–309.

36. Kaan TKY, Yip PK, Patel S, Davies M, Marchand F, Cockayne DA, Nunn PA, Dickenson AH, Ford APDW, Zhong Y, Malcangio M and McMahon SB. Systemic blockade of P2X3 and P2X2/3 receptors attenuates bone cancer pain behaviour in rats. *Brain* 2010; 133: 2549–2564.

37. King T, Vardanyan A, Majuta L, Melemedjian O, Nagle R, Cress AE, Vanderah TW, Lai J and Porreca F. Morphine treatment accelerates sarcoma-induced bone pain, bone loss, and spontaneous fracture in a murine model of bone cancer. *Pain* 2007; 132: 154–168.

38. Liu M, Yang H, Fang D, Yang J-J, Cai J, Wan Y, Chui D-H, Han J-S and Xing G-G. Upregulation of P2X3 receptors by neuronal calcium sensor protein VILIP-1 in dorsal root ganglions contributes to the bone cancer pain in rats. *Pain* 2013; 154: 1551–1568.

39. Scott AC, McConnell S, Laird B, Colvin L and Fallon M. Quantitative Sensory Testing to assess the sensory characteristics of cancer-induced bone pain after radiotherapy and potential clinical biomarkers of response. *Eur J Pain* 2012; 16: 123–133.

40. Wu JX, Xu MY, Miao XR, Lu ZJ, Yuan XM, Li XQ and Yu WF. Functional up-regulation of P2X3 receptors in dorsal root ganglion in a rat model of bone cancer pain. *Eur J Pain Lond Pain* 2012; 16: 1378–1388.

41. Zhou Y-L, Jiang G-Q, Wei J, Zhang H-H, Chen W, Zhu H, Hu S, Jiang X and Xu G-Y. Enhanced binding capability of nuclear factor-κB with demethylated P2X3 receptor gene contributes to cancer pain in rats. *Pain* 2015; 156: 1892–1905.

42. Amaya F, Wang H, Costigan M, Allchorne AJ, Hatcher JP, Egerton J, Stean T, Morisset V, Grose D, Gunthorpe MJ, Chessell IP, Tate S, Green PJ and Woolf CJ. The voltage-gated sodium channel Na(v)1.9 is an effector of peripheral inflammatory pain hypersensitivity. *J Neurosci* 2006; 26: 12852–12860.

43. Katz EJ and Gold MS. Inflammatory hyperalgesia: a role for the C-fibre sensory neuron cell body? *J Pain* 2006; 7: 170–178.

44. Liu CN, Wall PD, Ben-Dor E, Michaelis M, Amir R and Devor M. Tactile allodynia in the absence of C-fibre activation: altered firing properties of DRG neurons following spinal nerve injury. *Pain* 2000; 85: 503–521.

45. Schaible HG. Peripheral and central mechanisms of pain generation. *Handb Exp Pharmacol* 2007; 177: 3–28.

46. Yang R-H, Xing J-L, Duan J-H and Hu S-J. Effects of gabapentin on spontaneous discharges and subthreshold membrane potential oscillation of type A neurons in injured DRG. *Pain* 2005; 116: 187–193.

47. Kuner R. Central mechanisms of pathological pain. *Nat Med* 2010; 16: 1258–1266.

48. Woolf CJ and Salter MW. Neuronal plasticity: increasing the gain in pain. *Science* 2000; 288: 1765–1769.

49. Khasabov SG, Hamamoto DT, Harding-Rose C and Simone DA. Tumour-evoked hyperalgesia and sensitization of nociceptive dorsal horn neurons in a murine model of cancer pain. *Brain Res* 2007; 1180: 7–19.

50. Koerber HR, Mirnics K, Brown PB and Mendell LM. Central sprouting and functional plasticity of regenerated primary afferents. *J Neurosci* 1994; 14: 3655–3671.

51. Lekan HA, Carlton SM and Coggeshall RE. Sprouting of A beta fibres into lamina II of the rat dorsal horn in peripheral neuropathy. *Neurosci Lett* 1996; 208: 147–150.

52. Nakamura S and Myers RR. Myelinated afferents sprout into lamina II of L3-5 dorsal horn following chronic constriction nerve injury in rats. *Brain Res* 1999; 818: 285–290.

53. Woolf CJ, Shortland P and Coggeshall RE. Peripheral nerve injury triggers central sprouting of myelinated afferents. *Nature* 1992; 355: 75–78.

54. Woolf CJ, Shortland P, Reynolds M, Ridings J, Doubell T and Coggeshall RE. Reorganization of central terminals of myelinated primary afferents in the rat dorsal horn following peripheral axotomy. *J Comp Neurol* 1995; 360: 121–134.

55. Phokeo V, Kwiecien JM and Ball AK. Characterization of the optic nerve and retinal ganglion cell layer in the dysmyelinated adult Long Evans Shaker rat: evidence for axonal sprouting. *J Comp Neurol* 2002; 451: 213–224.

56. Kwiecien JM. Cellular compensatory mechanisms in the CNS of dysmyelinated rats. *Comp Med* 2010; 60: 205–217.

57. Kwiecien JM and Avram R. Long-distance axonal regeneration in the filum terminale of adult rats is regulated by ependymal cells. *J Neurotrauma* 2008; 25: 196–204.

58. Mantyh PW. The neurobiology of skeletal pain. *Eur J Neurosci* 2014; 39: 508–519.

59. Guan X, Fu Q, Xiong B, Song Z, Shu B, Bu H, Xu B, Manyande A, Cao F and Tian Y. Activation of PI3Kγ/Akt pathway mediates bone cancer pain in rats. *J Neurochem* 2015; 134: 590–600.

60. Hu X-M, Liu Y-N, Zhang H-L, Cao S-B, Zhang T, Chen L-P and Shen W. CXCL12/CXCR4 chemokine signaling in spinal glia induces pain hypersensitivity through MAPKs-mediated neuroinflammation in bone cancer rats. *J Neurochem* 2015; 132: 452–463.

61. Wall PD and Woolf CJ. Muscle but not cutaneous C-afferent input produces prolonged increases in the excitability of the flexion reflex in the rat. *J Physiol* 1984; 356: 443–458.

62. Woolf CJ. Evidence for a central component of post-injury pain hypersensitivity. *Nature* 1983; 306: 686–688.